Progress In Electromagnetics Research, Vol. 136, 61–77, 2013

COMPUTATIONAL PERFORMANCE OF A WEIGHTED REGULARIZED MAXWELL EQUATION FINITE ELEMENT FORMULATION

Ruben Otin[1, *], Luis E. Garcia-Castillo[2], Ignacio Martinez-Fernandez[2], and Daniel Garcia-Doñoro[2]

[1]Centre Internacional de Mètodes Numèrics en Enginyeria (CIMNE), Parque Mediterráneo de la Tecnología, Edificio C3, Oficina 206, Castelldefels, Barcelona 08860, Spain

[2]Dep. Teoría de la Señal y Comunicaciones, Escuela Politécnica Superior, Universidad Carlos III de Madrid (UC3M), Avda. de la Universidad, 30-28911 Leganés, Madrid, Spain

Abstract—The aim of this work is to asses the computational performance of a finite element formulation based on nodal elements and the regularized Maxwell equations. We analyze the memory requirements and the condition number of the matrix when the formulation is applied to electromagnetic engineering problems. As a reference, we solve the same problems with the best known finite element formulation based on edge elements and the double curl Maxwell equations. Finally, we compare and discuss the computational efficiency of both approaches.

1. INTRODUCTION

In this work we analyze the computational performance of a finite element (FEM) formulation which solves numerically the regularized time-harmonic Maxwell equations using nodal elements. This formulation is described in [1]. There are several reasons to study this approach: It offers spurious-free solutions and well-conditioned matrices even at low frequencies [2, 3]. Only the three components of **E**, or **H**, are the unknowns (there is no need of extra functions such as Lagrange multipliers or scalar potentials [4]). Its integral representation has a singular kernel of order 1 (instead of the order 3 exhibited by the double-curl formulation), which makes the regularized

Received 20 August 2012, Accepted 5 January 2013, Scheduled 16 January 2013

* Corresponding author: Ruben Otin (rotin@cimne.upc.edu).

formulation well suited for hybridization with integral numerical techniques [5–9]. The nodal solution of the electromagnetic problem is easy to couple in multiphysics problems (thermal, mechanic,...) which usually use nodal elements [10, 11]. Finally, we can also add to the list curiosity, because the weighted regularized formulation has not been properly investigated by the computational electromagnetic community.

But, despite all the advantages enumerated above, several drawbacks keeps this formulation out of the mainstream. The main drawback is the special treatment that must be given to the points of the domain where the field is singular and/or discontinuous [1]. This special treatment is what makes its software implementation and modeling more difficult than with the edge-based FEM formulations [12, 13] and what dissuades computational electromagnetic scientist from its use.

Therefore, although the regularized formulation had been applied successfully to a wide variety of problems (e.g., specific absorption rate computations [2, 14, 15], microwave engineering [1], electromagnetic compatibility [16], electromagnetic forming [3]) there is a question that remains unanswered: Is it worthy the investment of time and effort in the more complex implementation and modeling of the regularized formulation?. This is the question we try to answer in this work.

2. WEIGHTED REGULARIZED MAXWELL EQUATION WITH NODAL ELEMENTS

Solving the regularized Maxwell equations [5] is equivalent to finding $\mathbf{E} \in \mathbf{H}_0$ (**curl**, div; Ω) such that $\forall \mathbf{F} \in \mathbf{H}_0$ (**curl**, div; Ω) holds:

$$\int_\Omega \frac{1}{\mu} \ (\nabla \times \mathbf{E}) \cdot \left(\nabla \times \bar{\mathbf{F}}\right) \ + \ \int_\Omega \frac{1}{\mu\varepsilon\bar{\varepsilon}} \ (\nabla \cdot (\varepsilon \mathbf{E})) \cdot \left(\nabla \cdot \left(\bar{\varepsilon}\, \bar{\mathbf{F}}\right)\right) - \ \omega^2 \int_\Omega \varepsilon\, \mathbf{E} \cdot \bar{\mathbf{F}} \ + \ \mathbf{R.B.C.}|_{\partial\Omega} \ = \ i\omega \int_\Omega \mathbf{J} \cdot \bar{\mathbf{F}}, \tag{1}$$

where

$$\mathbf{H}_0\,(\mathbf{curl}, \mathrm{div}; \Omega) := \left\{\mathbf{F} \in \mathbf{L}^2(\Omega)\,|\nabla \times \mathbf{F} \in \mathbf{L}^2(\Omega), \ \ \nabla \cdot (\varepsilon \mathbf{F}) \in L^2(\Omega)\,, \ \ \hat{\mathbf{n}} \times \mathbf{F} = 0 \text{ in PEC}\right\},$$

$L^2(\Omega)$ is the space of square integrable functions in the domain Ω, $\mathbf{L}^2(\Omega)$ the space of vectorial functions with all its components belonging to $L^2(\Omega)$, $\partial\Omega$ the boundary of the domain Ω, PEC the perfect electric conductor boundary, $\hat{\mathbf{n}}$ the unit normal to a surface, μ the magnetic permeability, ε the electric permittivity, $i = \sqrt{-1}$ the imaginary unit,

ω the angular frequency, $\mathbf{J}$ an imposed current density, $\mathbf{R.B.C.}|_{\partial\Omega}$ the term, properly adapted to the regularization, that takes into account the boundary conditions, and the bar over a magnitude denotes its complex conjugate. Its general expression is

$$\begin{aligned}\mathbf{R.B.C.}|_{\partial\Omega} \;=\; & \int_{\partial\Omega} \frac{1}{\mu}\left(\hat{\mathbf{n}}\times\nabla\times\mathbf{E}\right)\cdot\bar{\mathbf{F}} \\ & -\int_{\partial\Omega} \frac{1}{\mu\varepsilon\bar{\varepsilon}}\left(\nabla\cdot(\varepsilon\mathbf{E})\right)\left(\hat{\mathbf{n}}\cdot\left(\bar{\varepsilon}\bar{\mathbf{F}}\right)\right). \end{aligned} \tag{2}$$

On the surface of a perfect electric conductor (PEC) we impose the regularized version of the standard PEC boundary condition [5]

$$\begin{aligned}\nabla\cdot(\varepsilon\mathbf{E}) &= 0, \\ \hat{\mathbf{n}}\times\mathbf{E} &= 0,\end{aligned} \tag{3}$$

On a boundary simulating a surface at infinity we impose the regularized version [5] of the first order absorbing boundary condition (1stABC)

$$\begin{aligned}\hat{\mathbf{n}}\times\nabla\times\mathbf{E} &= i\omega\sqrt{\epsilon_0\mu_0}\left(\hat{\mathbf{n}}\times\hat{\mathbf{n}}\times\mathbf{E}\right), \\ \nabla\cdot\mathbf{E} &= i\omega\sqrt{\epsilon_0\mu_0}\left(\hat{\mathbf{n}}\cdot\mathbf{E}\right).\end{aligned} \tag{4}$$

On the surface of a waveguide port with only the fundamental mode propagating (e.g., TE_{10} in a rectangular waveguide, TEM in a coaxial waveguide) we impose [12, 17]

$$\begin{aligned}\hat{\mathbf{n}}\times\nabla\times\mathbf{E} &= \gamma\left(\hat{\mathbf{n}}\times\hat{\mathbf{n}}\times\mathbf{E}\right)+\mathbf{U}, \\ \hat{\mathbf{n}}\cdot\mathbf{E} &= 0,\end{aligned} \tag{5}$$

where γ is the propagation constant of the fundamental mode $\mathbf{E}_{fm}$ and

$$\begin{aligned}\mathbf{U} &= -2\,\gamma\left(\hat{\mathbf{n}}\times\hat{\mathbf{n}}\times\mathbf{E}_{fm}\right), \\ \mathbf{U} &= 0\end{aligned} \tag{6}$$

for the input and the output port, respectively (see [2] for more details).

In [5] it is demonstrated the equivalence of the above formulation with the Maxwell equations and the absence of spurious solutions when it is solved using nodal finite elements. In [5, 17] it is also shown that the extended boundary conditions (3) to (5) are necessary to have a well-posed problem. To implement the boundary conditions we only have to impose the Dirichlet conditions ($\hat{\mathbf{n}}\times\mathbf{E}=0$ or $\hat{\mathbf{n}}\cdot\mathbf{E}=0$) with the techniques explained in [17] and substitute the rest of the equalities in the $\mathbf{R.B.C.}|_{\partial\Omega}$ term defined in (2).

But, as shown in [18], if the analytical solution of the Maxwell equations is singular at some point of the domain (as can happen, for instance, in a PEC re-entrant corner [19]) we can not approximate

this analytical solution with nodal elements and the regularized formulation. This problem caused by the field singularities is overridden in [18] by applying a weight in the divergence term of (1). This weight depends on the order of the singularity [19] and tends to zero when approaching to it.

In this work, we follow the approach explained in [1], which is a simplification of the method developed in [18]. The simplified approach [1] consists in removing the divergence term of (1) in a few layers of elements around the singularity. In [1, 2, 6] it is shown that accurate solutions can be obtained with second order tetrahedral nodal elements if we cancel the divergence term in three layers. That is, we must cancel the divergence term in the elements with a node resting on reentrant corners and edges of PECs, corners and edges of dielectrics and on the intersection of several dielectrics [19]. We also have to cancel the divergence term in the elements which are in contact with the previous elements and in the elements which are in contact with these (3 layers). In [1] it is also explained the strategy to follow when the field is discontinuous at the surfaces separating two different materials or at the intersection of three or more different materials.

The above simplified formulation has been implemented in an in-house code called ERMES (*E*lectric *R*egularized *M*axwell *E*quations with *S*ingularities). ERMES [20] has an user-friendly interface based on the commercial software GiD [21]. GiD is employed for geometrical modeling, meshing and visualization of results. From the graphical interface of GiD we obtain the elements and nodes which need a special treatment. Then, ERMES, thanks to its C++ object oriented implementation, is able to manage easily all the different types of elements present in the regularized formulation.

Previous nodal-based approaches (double-curl formulation with nodal elements) produced spurious solutions because they do not guarantee a null divergence in the resultant discretized fields. Therefore, its nodal discretization provided non-physical solutions which were not a good numerical approximation of the original set of Maxwell equations. It was necessary to use curl-conforming elements with the double-curl formulation to obtain a discrete null divergence solution (in a weak sense).

On the other hand, the penalized nodal-based approaches impose explicitly in its formulation the null-divergence with an arbitrary weighted divergence term in its weak form. But, they ignore some extra boundary conditions which are necessary to set a well-posed problem equivalent to the original Maxwell equations [5]. Also, they ignore that we must take special care of the field singularities when imposing the null-divergence. If the field is singular, the solution obtained with

the penalized formulation can be globally wrong independently of the mesh size or the polynomial order used in the discretization.

In some specific situations (for instance, in a problem with all the boundaries PEC), the penalized formulations can be equivalent to regularized formulation. Then, in both cases, if we do not pay attention to the field singularities, wrong solutions can be obtained. In these circumstances, the reason behind the wrong solution is not the non-null divergence problem explained above. The real causa is the non-density of the space spanned by the nodal basis inside $\mathbf{H}_0$ (**curl**, div; Ω) in non-convex polyhedral domain (see [18]). Sometimes, the wrong solutions obtained with penalized nodal-based approaches in these domains were erroneously attributed to non-null divergence spurious modes instead to the presence of field singularities.

The main differences of the formulation proposed in this work with other nodal-based formulations is the way it imposes the null-divergence of the fields and the special treatment given to the singularities. The regularized formulation [5] imposes explicitly a control over the divergence of the fields by means of the divergence term appearing in the weak form (1) and the extended boundary conditions (3) to (5). No extra unknowns (such as Lagrange multipliers) or arbitrary weights are required. The extra term plus the extended boundary conditions guarantee that the solution has a null divergence and, therefore, it is free of spurious non-physical modes. Moreover, we have added a weight function to the divergence term [18, 1], that makes possible to converge to the physical solution even when the field has a singularity.

The problem with the singularities is really a very peculiar and unexpected problem. If you solve the regularized formulations without taking care of the singularities you obtain solutions that, at first sight, seem physically sounded but, that, after a more careful examination, are globally wrong. Although, initially, you can think that the reason is only a code bug or a spurious solution, the real reason rests deep inside the functional framework of the regularized formulation. In [18, 1] are exposed the reasons and solutions for this problem. Also, it can be found a compressive exposition of the problem in the review [22].

As is mentioned in Section 1, the method presented here has been validated in several applications but, of course, it is a rather new approach and requires further research. In this paper, what we try to evaluate is that if it is worthy to keep up with this research and if it is profitable the extra effort of its more involved implementation and modeling when we compare its computational performance with the best known edge-based double-curl formulation.

3. CURL-CURL MAXWELL EQUATION WITH EDGE ELEMENTS

Solving the curl-curl Maxwell equations is equivalent to finding $\mathbf{E} \in \mathbf{H}_0(\mathbf{curl}; \Omega)$ such that $\forall\, \mathbf{F} \in \mathbf{H}_0(\mathbf{curl}; \Omega)$ holds:

$$\int_\Omega \frac{1}{\mu}(\nabla \times \mathbf{E}) \cdot (\nabla \times \bar{\mathbf{F}}) - \omega^2 \int_\Omega \varepsilon \mathbf{E} \cdot \bar{\mathbf{F}} + \mathbf{B.C.}|_{\partial\Omega} = i\omega \int_\Omega \mathbf{J} \cdot \bar{\mathbf{F}}, \quad (7)$$

where

$$\mathbf{H}_0(\mathbf{curl}; \Omega) := \{\mathbf{F} \in \mathbf{L}^2(\Omega) | \nabla \times \mathbf{F} \in \mathbf{L}^2(\Omega), \quad \hat{\mathbf{n}} \times \mathbf{F} = 0 \text{ in PEC}\} \quad (8)$$

and $\mathbf{B.C.}|_{\partial\Omega}$ is the term that takes into account the boundary conditions. The rest of the notation is the same as in Section 2. The general expression for $\mathbf{B.C.}|_{\partial\Omega}$ is

$$\mathbf{B.C.}|_{\partial\Omega} = \int_{\partial\Omega} \frac{1}{\mu} (\hat{\mathbf{n}} \times \nabla \times \mathbf{E}) \cdot \bar{\mathbf{F}}. \quad (9)$$

On the surface of a perfect electric conductor (PEC) we impose

$$\hat{\mathbf{n}} \times \mathbf{E} = 0. \quad (10)$$

On a boundary simulating a surface at infinity we impose the the first order absorbing boundary condition (1stABC)

$$\hat{\mathbf{n}} \times \nabla \times \mathbf{E} = i\omega\sqrt{\epsilon_0 \mu_0}\, (\hat{\mathbf{n}} \times \hat{\mathbf{n}} \times \mathbf{E}). \quad (11)$$

On the surface of a waveguide port with only the fundamental mode propagating we impose

$$\hat{\mathbf{n}} \times \nabla \times \mathbf{E} = \gamma\, (\hat{\mathbf{n}} \times \hat{\mathbf{n}} \times \mathbf{E}) + \mathbf{U}, \quad (12)$$

where γ and $\mathbf{U}$ are the same as in Section 2.

The classical FEM approach in computational electromagnetics consists in solving the weak formulation (7) discretized with edge elements [12, 13]. In this work, we use this approach as a reference.

4. NUMERICAL EXPERIMENTS

We calculated the electric field for several electromagnetic engineering problems to test the computational performance of the nodal finite element formulation of Section 2 (RM-Nodal). As a reference, we computed identical problems using the curl-curl Maxwell formulation of Section 3 (CC-Edge) with the same geometry, mesh and boundary conditions.

All the geometries and meshes were generated with GiD version 10.0.5 for MS Windows 64 bits. These meshes were composed of tetrahedra. Curved elements (second order approximation for the

geometry) were used to fit curved boundaries. Also a second order of interpolation was used for the finite element basis (nodal basis functions [23] for the RM-Nodal formulation and curl conforming basis functions[24, 13] for the CC-Edge formulation).

The accuracy of the solutions was checked by comparing the results of both formulations between them and with those provided by a benchmark. We also used a direct solver to check that the matrices were correct. Once the accuracy of both approaches was guaranteed, we examined the following parameters:

- Degrees of freedom (DOF): number of unknowns (complex numbers) of the linear system.
- Non-zero entries (Non-Zero): number of elements (complex numbers) of the matrix with an absolute value higher than $1e-16$.
- Peak memory usage (RAM): maximum RAM memory (in kB) required by the solver.
- Number of iterations (Iterations): number of iterations needed by the iterative solver to reach a residual $r = ||Ax - b||/||b||$ lower than $1e - 4$.
- Solver time (Time): time required (in seconds) to solve the linear system.

There are no data regarding the building of the matrices because no significant differences were observed between the RM-Nodal and the CC-Edge formulations.

The matrices were symmetric in all the problems analyzed, therefore, only the diagonal and the upper half of the matrices were considered for computation. The linear systems were solved with a quasi-minimal residual (QMR) iterative solver [25] and a diagonal preconditioner. The number of iterations needed by the QMR to reach convergence was employed as an indicative measure of the condition number of the matrices.

We also tested the conjugate gradient (CG) and the bi-conjugate gradient (BiCG) solvers with a diagonal preconditioner. We observed that the BiCG always converged faster than the CG despite the oscillating value of the BiCG residual with the number of iterations. Nevertheless, the use of the CG or the BiCG did not change the relative number of iterations required to solve the matrix of one formulation to respect the other. The reason to choose the QMR was because it converged in a similar time and number of iterations than the BiCG but with a steady decreasing of the residual. This feature makes easier the prediction of its behavior.

The desktop computer utilized for the numerical experiments had a CPU Intel Core 2 Quad Q9300 at 2.5 GHz, 8 GB of RAM memory and

the operative system Microsoft Windows XP Professional x64 Edition v2003. In the following we describe four representative examples of all the simulations performed.

4.1. Ellipsoidal Phantom in Waveguide

In this example we computed the specific absorption rate (SAR) of an ellipsoidal phantom placed inside a rectangular waveguide (see Fig. 1). The ellipsoidal phantom is filled with a substance of electrical permittivity $\epsilon = 43\epsilon_0$ and conductivity $\sigma = 0.97\,\mathrm{S/m}$. The phantom is placed at the center of a rectangular waveguide WR-975 and illuminated with the fundamental mode TE_{10} at the frequency $f = 900\,\mathrm{MHz}$. This experimental set-up is similar to those typically found when studying the effect of radiation on small animals or biological samples [26–28]. More details about the FEM modeling and validation of results can be found in [2]. The computational parameters obtained for this example are shown in Table 1.

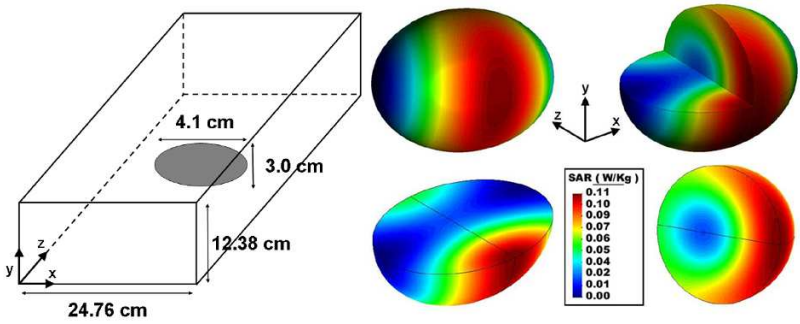

Figure 1. Geometry set-up and SAR computed with ERMES for the ellipsoidal phantom inside a rectangular waveguide. Results validated in [2].

Table 1. Computational parameters obtained for the ellipsoidal phantom inside a rectangular waveguide. The FEM mesh was composed of 146 558 isoparametric second order tetrahedral elements.

	DOF	Non-Zero	RAM (kB)	Iterations	Time (s)
CC-Edge	947 280	19 988 350	780 176	107 941	34 308
RM-Nodal	581 167	23 300 611	808 444	726	179

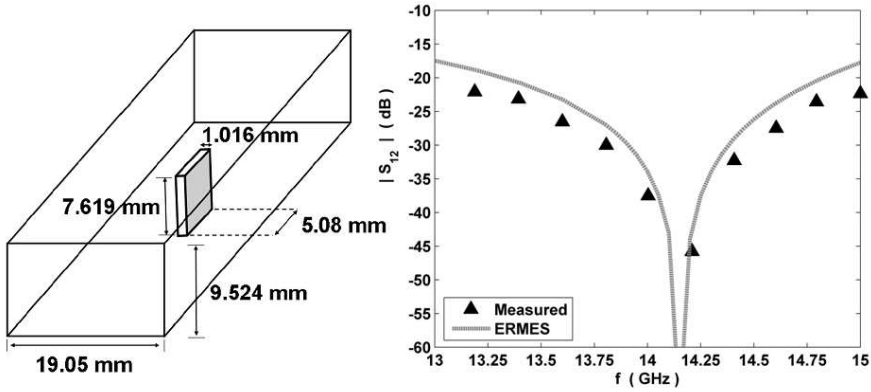

Figure 2. Geometry set-up and transmission coefficient for the ridge waveguide. The results obtained with ERMES are compared with the measurements performed in [29].

Table 2. Computational parameters obtained for the ridge waveguide. The FEM mesh was composed of 210 757 isoparametric second order tetrahedral elements.

	DOF	Non-Zero	RAM (kB)	Iterations	Time (s)
CC-Edge	1 425 208	26 121 205	1 055 336	189 750	95 260
RM-Nodal	813 276	30 512 483	1 068 536	1 113	372

4.2. Ridge Waveguide

In this example we calculated the fields for the ridge waveguide shown in Fig. 2 at the frequency $f = 14.15\,\text{GHz}$. The computational parameters obtained are shown in Table 2.

4.3. PMR Antenna near SAM Head

In this example we computed the SAR produced by a professional mobile radio (PMR) antenna in a specific anthropomorphic mannequin (SAM) head (see Figures 3 and 4). The PMR antenna was fed with $P_0 = 2\,\text{W}$ at a frequency of $f = 390\,\text{MHz}$. The mass density of the SAM head was $\rho = 1000\,\text{kg/m}^3$, and its electrical properties were $\epsilon = 45.5\epsilon_0$ and $\sigma = 0.7\,\text{S/m}$. More details about the FEM modeling a validation can be found in [2]. The computational parameters obtained for this example are shown in Table 3.

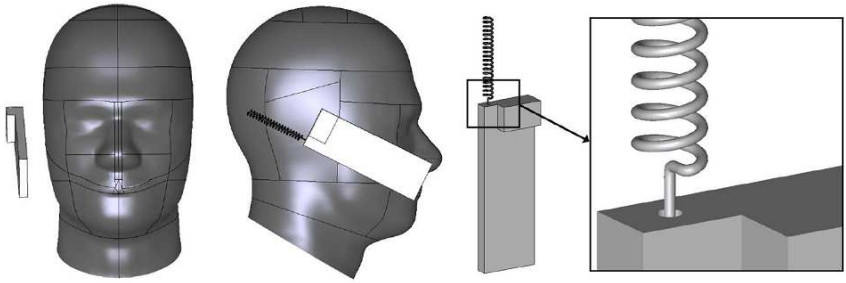

Figure 3. Geometry set-up for the PMR antenna near SAM head and detail of the coaxial feeding.

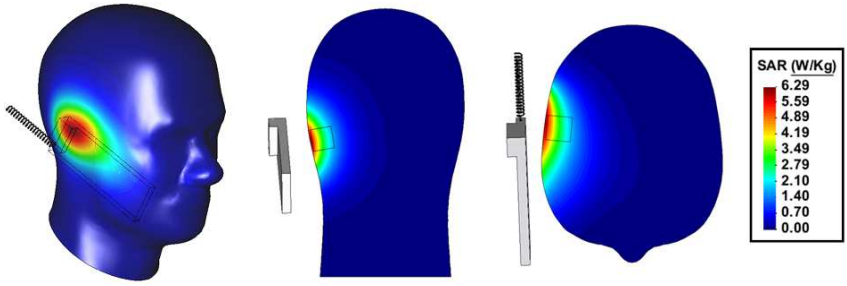

Figure 4. SAR distribution calculated with ERMES. Results validated in [2].

Table 3. Computational parameters obtained for the PMR antenna near SAM head. The FEM mesh was composed of 508 690 isoparametric second order tetrahedral elements.

	DOF	Non-Zero	RAM (kB)	Iterations	Time (s)
CC-Edge	3 386 960	75 259 074	2 655 368	$>$ 400 000	-
RM-Nodal	1 992 795	77 299 993	2 712 008	8 158	7 477

4.4. Hemispherical Dielectric Resonator Antenna

In this example we calculated the electric field at the frequency $f = 3.65\,\text{GHz}$ for the hemispherical dielectric resonator antenna described in [30] (see Figures 5 and 6). The computational parameters obtained for this example are shown in Table 4.

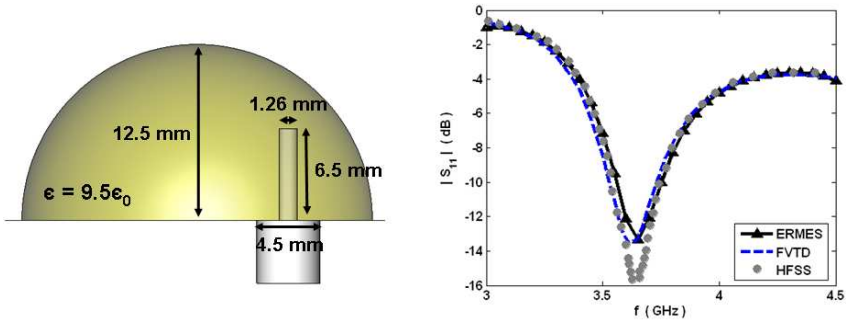

Figure 5. Geometry set-up and reflection coefficient for the hemispherical dielectric resonator antenna. ERMES results are compared with the simulations performed in [30].

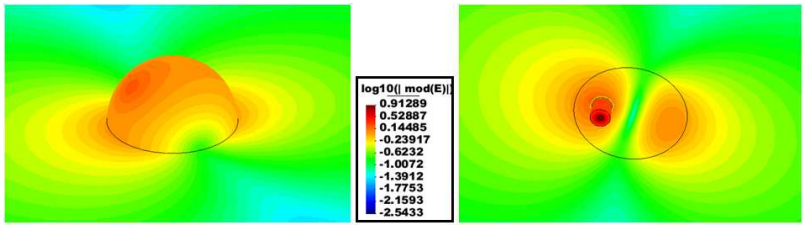

Figure 6. Electric field at $f = 3.65\,\text{GHz}$ calculated with ERMES for the hemispherical dielectric resonator antenna.

Table 4. Computational parameters obtained for the hemispherical dielectric resonator antenna. The FEM mesh was composed of 822 938 isoparametric second order tetrahedral elements.

	DOF	Non-Zero	RAM (kB)	Iterations	Time (s)
CC-Edge	5 340 766	131 010 032	4 482 088	$> 400\,000$	-
RM-Nodal	3 300 646	133 288 543	4 581 160	4 787	8 807

5. SUMMARY

The numerical experiments of Section 4 show that, for a given mesh, the DOFs in the CC-Edge formulation are almost twice the DOFs in the RM-Nodal formulation. However, the number of non-zero entries in a CC-Edge matrix is only slightly smaller than the number of non-zero

Table 5. Peak RAM memory usage (kB) for the examples of Section 4.

	Ellipsoidal phantom	Ridge waveguide	PMR near SAM head	Dielectric antenna
CC-Edge	780 176	1 055 336	2 655 368	4 482 088
RM-Nodal	808 444	1 068 536	2 712 008	4 581 160

Table 6. Number of iterations needed by the diagonal preconditioned QMR solver to reach convergence in the examples of Section 4.

	Ellipsoidal phantom	Ridge waveguide	PMR near SAM head	Dielectric antenna
CC-Edge	107 941	189 750	$> 400\,000$	$> 400\,000$
RM-Nodal	726	1 113	8 158	4 787

entries in a RM-Nodal matrix. Therefore, we have different sparsity patterns but similar memory requirements, as shown in Table 5.

On the other hand, the number of iterations of the QMR solver presents large differences (see Table 6). Clearly, the CC-Edge formulation needs to improve the solving technique (using Lagrange multipliers to stabilize the solution or a better preconditioning [31, 32, 22] or direct methods [33]) but, of course, at the cost of increasing the computational demands. By contrast, the RM-Nodal formulation is able to solve the problems effectively with a very simple iterative solver (as it is also shown in [2, 14, 1, 16]). This demonstrates the well-conditioning of the RM-Nodal matrices stated in Section 1.

In Table 6 we can also observe the effect of the singularities in the RM-Nodal formulation. Although the last example has more unknowns than the PMR-SAM head example, it converges in less iterations because it has fewer singular points. Nevertheless, the number of iterations remains under practical levels even in the presence of singularities [2].

Also there are differences in the values of the time per iteration (see Table 7). The reason behind these differences seems to be the sparsity patterns produced by each formulation. The RM-Nodal matrices have less rows but with more non-zeros per row than the CC-Edge matrices. When the sparse-matrix vector multiplication is carried out with the RM-Nodal sparsity pattern, it incurs in much less loop overhead (i.e., branch instructions) per floating point operation. We believe that

Table 7. Time per iteration (time (s)/iterations).

	Ellipsoidal phantom	Ridge waveguide	PMR near SAM head	Dielectric antenna
CC-Edge	0.3178	0.5020	-	-
RM-Nodal	0.2466	0.3342	0.9165	1.8398

is the most contributing factor to the observed differences in the computational times.

More examples of similar characteristics were solved, and in all the cases, the same pattern was observed for the computational parameters. The well-conditioning of the RM-Nodal matrices remained for bigger problems and even when the meshes had element sizes differences of several orders of magnitude. For instance, the RM-Nodal formulation can converge in less than 5000 QMR iterations in problems with more than $2e6$ second order elements ($\sim 7e6$ unknowns in the RM-Nodal formulation, $\sim 12e6$ unknowns in the CC-Edge formulation) and element size differences of two orders of magnitude. The RM-Nodal formulation was also applied to the computing of eddy currents and Lorentz forces in the low frequency regime [3], retaining the same good behavior.

6. CONCLUSION

In this paper we have shown that the reward of spending time implementing and modeling with the RM-Nodal formulation is a well-conditioned matrix easily solvable with lightly preconditioned iterative solvers. This well-conditioning remains even in the presence of singularities, in meshes with large element sizes differences and, also, when solving low-frequency (quasi-static) problems. To minimize the drawback of the complex implementation and modeling we only have to use wisely the pre-processor. We can extract from the geometry (with the CAD and mesher software) the elements which need special treatment (elements with nodes near a singularity and/or resting on a discontinuity surface). Then, with the proper implementation, we can process independently each type of element without affecting the rest of the FEM code.

By contrast, the CC-Edge formulation displays an easier implementation and modeling but it requires more elaborate and hardware demanding solvers. It has been shown that the CC-Edge formulation needs stabilization terms (Lagrange multipliers or

potentials) and/or better preconditioning (e.g., Multi-grid methods) to solve its matrix with an iterative solver. These options represent an increase in the computational cost respect to the RM-Nodal formulation, which does not need neither extra terms nor heavy preconditioners.

Therefore, depending on our preferences, we can choose between the easy implementation and modeling featured by the CC-Edge formulation at the cost of requiring more expensive solvers, or, the easily solvable matrices produced by the RM-Nodal formulation at the cost of a more laborious implementation and modeling.

ACKNOWLEDGMENT

This work was partially funded by the European Research Council, FP7 Programme Ideas, Starting Grant 258443 — COMFUS (Computational Methods for Fusion Technology). The authors would also like to acknowledge the support of the Spanish Ministry of Science and Education under project TEC2010-18175/TCM.

REFERENCES

1. Otin, R., "Regularized Maxwell equations and nodal finite elements for electromagnetic field computations," *Electromagnetics*, Vol. 30, 190–204, 2010.
2. Otin, R. and H. Gromat, "Specific absorption rate computations with a nodal-based finite element formulation," *Progress In Electromagnetics Research*, Vol. 128, 399–418, 2012.
3. Otin, R., R. Mendez, and O. Fruitos, "A numerical model for the search of the optimum capacitance in electromagnetic metal forming," *The 8th International Conference and Workshop on Numerical Simulation of 3D Sheet Metal Forming Processes (NUMISHEET 2011), AIP Conference Proceedings*, Vol. 1383, 935–942, 2011.
4. Ciarlet, P., "Augmented formulations for solving Maxwell equations," *Computer Methods in Applied Mechanics and Engineering*, Vol. 194, 559–586, 2005.
5. Hazard, C. and M. Lenoir, "On the solution of the time-harmonic scattering problems for Maxwell's equations," *SIAM Journal on Mathematical Analysis*, Vol. 27, 1597–1630, 1996.
6. Bui, V. P., X. C. Wei, and E. P. Li, "An efficient simulation technology for characterizing the ultra-wide band signal propagation in a wireless body area network," *Journal of*

Electromagnetic Waves and Applications, Vol. 24, Nos. 17–18, 2575–2588, 2010.

7. Fernandez-Recio, R., L. E. Garcia-Castillo, S. Llorente-Romano, and I. Gomez-Revuelto, "Convergence study of a non-standard Schwarz domain decomposition method for finite element mesh truncation in electro-magnetics," *Progress In Electromagnetics Research*, Vol. 120, 439–457, 2011.
8. Bui, V. P., X.-C. Wei, E. P. Li, and W.-J. Zhao, "An efficient hybrid technique for analysis of the electromagnetic field distribution inside a closed environment," *Progress In Electromagnetics Research*, Vol. 114, 301–315, 2011.
9. Gomez-Revuelto, I., L. E. Garcia-Castillo, and L. F. Demkowicz, "A comparison between PML, infinite elements and an iterative BEM as mesh truncation methods for HP self-adaptive procedures in electromagnetics," *Progress In Electromagnetics Research*, Vol. 126, 499–519, 2012.
10. Cvetkovi, M., D. Poljak, and A. Peratta, "FETD computation of the temperature distribution induced into a human eye by a pulsed laser," *Progress In Electromagnetics Research*, Vol. 120, 403–421, 2011.
11. Mohsin, S. A., "Concentration of the specific absorption rate around deep brain stimulation electrodes during MRI," *Progress In Electromagnetics Research*, Vol. 121, 469–484, 2011.
12. Jin, J., *The Finite Element Method in Electromagnetics*, 2nd Edition, John Wiley & Sons, 2002.
13. Salazar-Palma, M., T. K. Sarkar, L.-E. García-Castillo, T. Roy, and A. Djordjevic, *Iterative and Self-adaptive Finite-elements in Electromagnetic Modeling*, Artech House Publishers, 1998.
14. Otin, R., "Numerical study of the thermal effects induced by a RFID antenna in vials of blood plasma," *Progress In Electromagnetics Research Letters*, Vol. 22, 129–138, 2011.
15. Gomez-Calero, C., N. Jamaly, L. Gonzalez, and R. Martinez, "Effect of mutual coupling and human body on MIMO performances," *The 3rd European Conference on Antennas and Propagation (EuCAP 2009)*, 1042–1046, 2009.
16. Otin, R., J. Verpoorte, and H. Schippers, "A finite element model for the computation of the transfer impedance of cable shields," *IEEE Transactions on Electromagnetic Compatibility*, Vol. 53, No. 4, 950–958, 2011.
17. Boyse, W. E., D. R. Lynch, K. D. Paulsen, and G. N. Minerbo, "Nodal-based finite-element modeling of Maxwell's equations,"

IEEE Transactions on Antennas and Propagation, Vol. 40, 642–651, 1992.

18. Costabel, M. and M. Dauge, "Weighted regularization of Maxwell equations in polyhedral domains," *Numerische Mathematik*, Vol. 93, No. 2, 239–277, 2002.
19. Bladel, J. V., *Singular Electromagnetic Fields and Sources*, IEEE Press, 1991.
20. Otin, R., "ERMES user guide," International Center for Numerical Methods in Engineering (CIMNE), Ref. IT-617, Tech. Rep., 2011.
21. GiD, "The personal pre and post processor," International Center for Numerical Methods in Engineering (CIMNE), Barcelona, Spain, 2012, Online Available: http://www.gidhome.com.
22. Hiptmair, R., "Finite elements in computational electromagnetism," *Acta Numerica*, Vol. 1, 237–339, 2002.
23. Zienkiewicz, O. C. and R. L. Taylor, *The Finite Element Method*, Butterworth-Heinemann, 2000.
24. García-Castillo, L. E. and M. Salazar-Palma, "Second-order Nédélec tetrahedral element for computational electromagnetics," *International Journal of Numerical Modelling: Electronic Networks, Devices and Fields*, Vol. 13, Nos. 2–3, 261–287, 2000.
25. Freund, R. W. and N. M. Nachtigal, "QMR: A quasi-minimal residual method for non-Hermitian linear systems," *SIAM Journal: Numerische Mathematik*, Vol. 60, 315–339, 1991.
26. Jorge-Mora, T., M. Alvarez-Folgueiras, J. Leiro, F. J. Jorge-Barreiro, F. J. Ares-Pena, and E. Lopez-Martin, "Exposure to 2.45 GHz microwave radiation provokes cerebral changes in induction of HSP-90 α/β heat shock protein in rat," *Progress In Electromagnetics Research*, Vol. 100, 351–379, 2010.
27. Angulo, L. D., S. G. Garcia, M. F. Pantoja, C. C. Sanchez, and R. G. Martin, "Improving the SAR distribution in Petri-dish cell cultures," *Journal of Electromagnetic Waves and Applications*, Vol. 24, Nos. 5–6, 815–826, 2010.
28. Trujillo-Romero, C. J., L. Leija, and A. Vera, "FEM modeling for performance evaluation of an electromagnetic oncology deep hyperthermia applicator when using monopole, inverted T, and plate antennas," *Progress In Electromagnetics Research*, Vol. 120, 99–125, 2011.
29. Mansour, R. R., R. S. K. Tong, and R. H. Machpie, "Simplified description of the field distribution in finlines and ridge waveguides and its application to the analysis of E-plane discontinuities,"

IEEE Transactions on Microwave Theory and Techniques, Vol. 36, No. 12, 1825–1832, 1988.

30. Baumann, D., C. Fumeaux, P. Leuchtmann, and R. Vahldieck, "Finite-volume time-domain (FVTD) method and its application to the analysis of hemispherical dielectric-resonator antennas," *IEEE MTT-S International Microwave Symposium Digest*, Vol. 2, 985–988, 2003.
31. Aghabarati, A. and J. P. Webb, "Auxiliary space preconditioning for hierarchical elements," *The 11th International Workshop on Finite Elements for Microwave Engineering (FEM2012)*, Estes Park, Colorado, USA, 2012.
32. Ledger, P. D. and K. Morgan, "The application of the HP-finite element method to electromagnetic problems," *Archives of Computational Methods in Engineering*, Vol. 12, No. 3, 235–302, 2005.
33. Garcia-Donoro, D., I. Martinez-Fernandez, L. E. Garcia-Castillo, Y. Zhang, and T. K. Sarkar, "RCS computation using a parallel in-core and out-of-core direct solver," *Progress In Electromagnetics Research*, Vol. 118, 505–525, 2011.